NANO LETTERS

Letter

pubs.acs.org/NanoLett

Directing Self-Assembly of DNA Nanotubes Using Programmable Seeds

Abdul M. Mohammed[†] and Rebecca Schulman*[,†,‡]

[†]Chemical and Biomolecular Engineering and [‡]Computer Science, Johns Hopkins University, Baltimore, Maryland 21218, United States

Supporting Information

ABSTRACT: Control over when and where nanostructures arise is essential for the self-assembly of dynamic or multicomponent devices. We design and construct a DNA origami seed for the control of DAE-E tile DNA nanotube assembly. Seeds greatly accelerate nanotube nucleation and growth because they serve as nanotube nucleation templates. Seeds also control nanotube circumference. Simulations predict nanotube growth rates and suggest a small nucleation barrier remains when nanotubes grow from seeds.

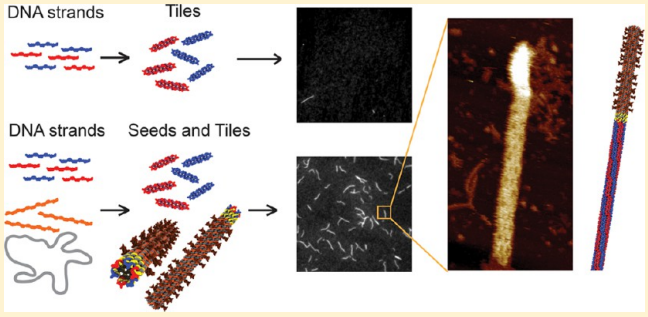

KEYWORDS: *DNA nanotubes, DNA origami, self-assembly, programmable nanostructures, controlling nanotube growth, programming nanotube circumference*

Creating structures and materials with defined molecular scale features is a major challenge in nanotechnology. It is difficult to use top-down fabrication methods to fabricate structures with nanoscale (10−50 nm) resolution or with three-dimensional structure; the development of strategies for self-assembly of structures of these types is therefore important. Self-assembled nanotubes made from carbon,[1−4] peptide,[5,6] and DNA have been considered as possible nanowires or templates for nanowires, structural filaments in roles analogous to the role of filaments in the cytoskeleton and may be useful substrates for active materials with controlled nanoscale motion, dynamics, and reconfiguration.[7−12] The specificity of DNA hybridization and the predictable, sequence-independent structure of the DNA double helix have enabled particularly precise control of nanotube structure,[13,14] chirality,[15] circumference,[16,17] and length.[18] The functionalization of DNA nanotubes mean that they may also serve as templates for the assembly of other materials.[19−22]

Many of the important potential applications of nanotubes are those in which nanotubes could serve as building blocks within larger structures. Engineered structures such as electronic circuits and biological structures such as the cytoskeleton are suggestive of the power of assemblies in which filaments or wires are precisely arranged. To use DNA nanotubes as building blocks for the construction of complex devices and structures, control over nanotube structure, where nanotubes are placed within a larger structure[23] and when nanotubes grow is required. One way to control both where and when a nanotube grows is by using a nucleating structure from which nanotube growth is initiated. If growth of nanotubes occurs readily from a nucleating structure but is otherwise rare, spatial and temporal control over nanotube growth could be achieved by controlling where such templates are placed and when they are present. Here we report templated DNA nanotube growth using a designed, rigid template that efficiently directs nanotube nucleation during annealing and isothermal growth and determines nanotube circumference.

DNA tiles[24,25] are versatile nanoscale building materials. Tiles have a well-defined structure and specific sequences (sticky ends) that can be programmed to hybridize to other tiles to form an extended structure. The tile type used in this study, the DAE-E DNA tile, consists of five short DNA strands that self-assemble to form a rigid tile structure (Figure 1a) because of a preference for Watson−Crick complementarity. During a typical annealing reaction DAE-E tiles first self-assemble from strands; tiles then self-assemble into lattices (Figure 1c). These lattices cyclize to form nanotubes (Figure 1d) due to the inherent curvature of tiles (150 ± 10°), which is equal to the minor groove angle of the DNA double helix.[13] Here we study nanotubes consisting of two DAE-E DNA tiles, each having different DNA sequences (Figure 1b).

Our goal was to control when and where nanotubes assemble by controlling when and where nucleation occurs. At low supersaturation, tile attachment by one sticky end is not energetically favorable, whereas attachment by 2 (or more) sticky ends is favorable. The formation of new nanotubes via homogeneous nucleation at low supersaturation is therefore

Received: March 8, 2013
Revised: July 8, 2013
Published: August 6, 2013

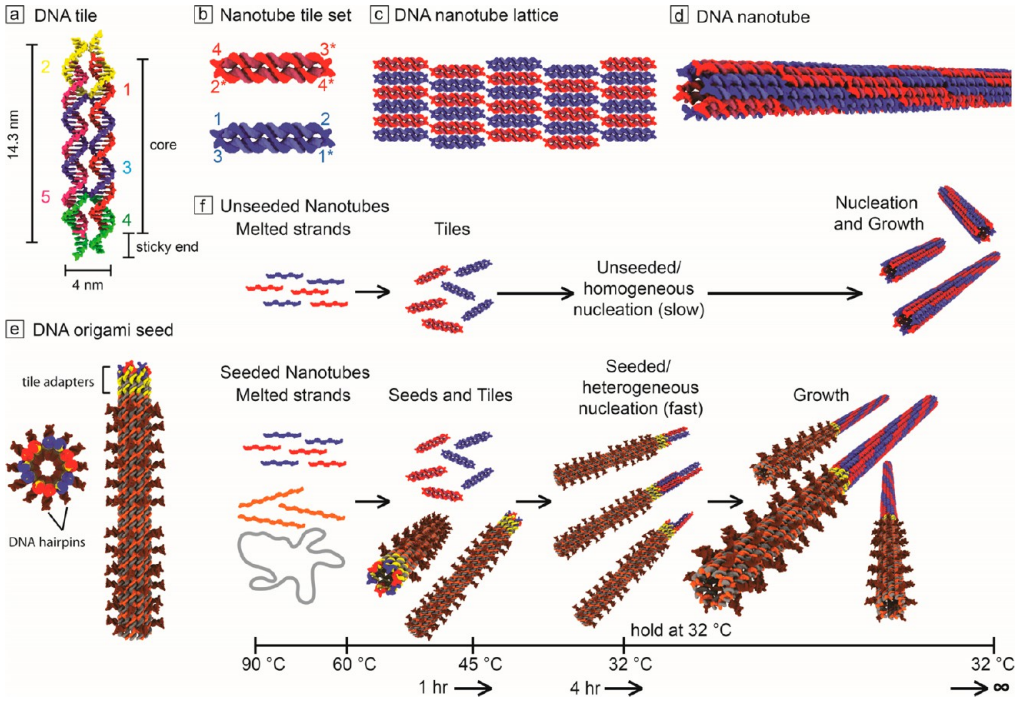

Figure 1. Schematic of the design of nanotubes, seeds, and the growth process. (a) DAE-E DNA tiles consist of five DNA strands, each shown in a different color. (b) The nanotube tile set has two types of tiles (red and blue) that have different core and sticky ends sequences. X* is complementary to X. (c) During self-assembly, tile sticky ends hybridize to form a larger lattice. The sticky end design in (b) produces diagonally stripped lattices. (d) The lattices in (c) cyclize into tubes. The tile design constrains nanotube circumferences to even numbers of tiles. (e) DNA origami seed. The seed consists of a scaffold strand (M13mp18), 72 staple strands that fold a long M13-single DNA into a cylinder shape, and 24 tile adapter strands that form a facet onto which nanotube tiles can attach. DNA hairpins on the outside of the cylinder are designed to force the seed to cyclize in a particular orientation. (f) The nanotube assembly process. At high temperatures, the tiles and seeds form. On the basis of the absence or presence of seeds, there are two pathways for nucleation. In unseeded nucleation, a homogeneous nucleus is formed from self-assembling tiles and subsequent tiles assemble to form nanotubes. During seeded nucleation, tiles polymerize on seeds, producing nanotubes. At low supersaturation, seeded nucleation is much faster than unseeded nucleation.

expected to be slow because the nucleation process requires several energetically unfavorable assembly steps.[13,26] A seed, a stable version of the critical nucleating structure for nanotubes, could reduce this barrier to nucleation by serving as a stable nucleus from which nanotubes can grow with no uphill assembly steps. During growth of tiles with seeds under low supersaturation conditions, almost all nanotubes would assemble from seeds, where there is little or no barrier to nanotube nucleation, rather than nucleating homogeneously (without seeds), which requires overcoming a significant energy barrier.

In this paper, we describe a strategy to direct DNA nanotube growth under low supersaturation conditions using designed seeds. We design and characterize a seed structure on which DNA nanotube tiles can assemble to nucleate a nanotube. Measurements of nanotube growth show that the presence of seeds increases the number of nanotubes that grow and the total length of nanotubes, suggesting that seeds reduce the barrier to nucleation. The seed is designed to act as a template for nanotube circumference, and we find that nanotubes that grow in the presence of seeds have the circumference that the seeds template. Our simulations suggest that the energetic barrier to nucleation is greatly reduced (but not eliminated) for DNA nanotube tiles assembling on seeds. Modeling also quantitatively predicts the number and length of nanotubes that arise without a parameter fit and identifies effects that are important to determining the outcome of the seeded growth process. Collectively, these results suggest that nanotube nucleation and growth are well understood processes and amenable to quantitative, rational control.

To build the seed, a thermally stable structure with a facet similar to a nanotube facet, we used the DNA origami technique, which involves folding of a long scaffold strand using many short staples strands into a specified shape.[27,28] The designed seed consists of 12 parallel DNA helices connected by crossover points between the helices. The helices are arranged in a cylindrical structure, similar to the arrangement of helices in a DAE-E tile nanotube. DNA hairpins within the staple strands were designed to fold on the surface of the seed designated as the outer surface. The hairpins were used to control the direction of cyclization: steric hindrance would prevent the seed from cyclizing with the hairpins inside the structure. Controlling the direction of seed cyclization is essential, as the direction of curvature of seeds needs to match the direction of curvature of the nanotubes. About one-third of the long scaffold strand was used to construct the designed seed and the remaining unused scaffold strand was left single stranded. To create a facet on the seed that directly resembles the crossover structure of DAE tile nanotubes (Supporting Information Figure 1), we designed a set of "adapter tiles"[29] (Supporting Information Figure 5) that bind on one side of the seed having the same crossover structure and sticky ends as DNA tile nanotubes.

Seeds Form As Designed. We used atomic force microscopy (AFM) to characterize the structure of folded seeds (Figure 2a,d,g). The cylindrical seeds measured 63.1 ±

dx.doi.org/10.1021/nl400881w | Nano Lett. 2013, 13, 4006−4013

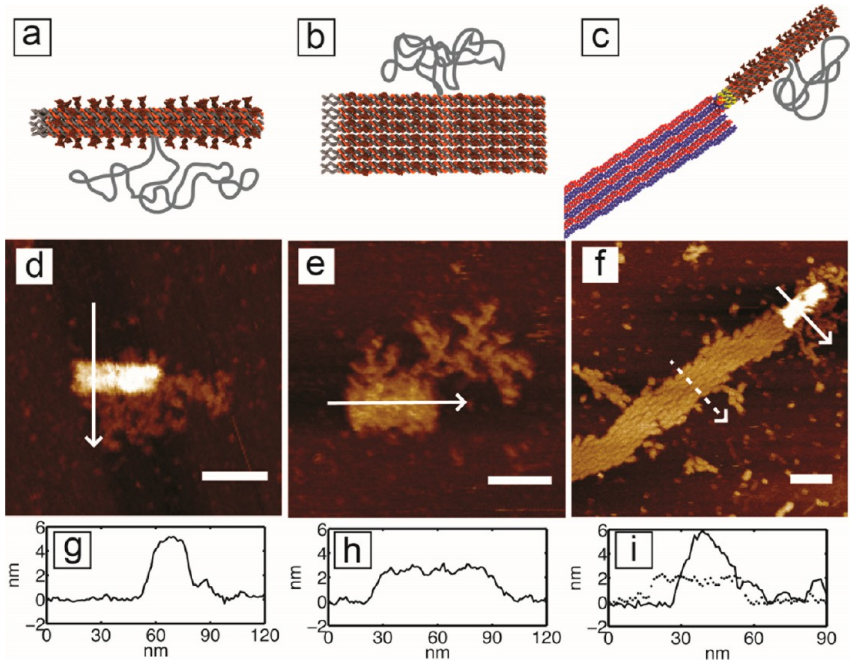

Figure 2. Seed structure and nanotube attachment. (a–c) Models showing top view of a seed origami, unrolled seed origami and seeded nanotube respectively. The entangled single-stranded DNA (gray) represents the unused part of the M13 strand and is not to scale. (d) AFM image of a folded seed, 63.1 ± 1.8 nm × 21.3 ± 1.4 nm. (e) AFM image of an unrolled seed, 65 ± 2.2 nm × 37.6 ± 1.0 nm from which the staples that connect helix 1 and helix 12 are excluded. (f) AFM image of a seeded nanotube. The interaction between the DNA and mica surface forces the nanotube to open into a lattice; seeds do not open on the mica surface because opening the seed would require dehybridizing staples from three adjacent DNA helices as compared to simply dehybridizing individual nanotube sticky ends. Scale bars 50 nm in d–f. (g–i) The section height profiles of a seed, unrolled seed, and seed with attached nanotube, respectively. The height of the seeded nanotube in (i) is represented by the dashed curve.

1.8 nm in length (expected length based on 3.6 nm/turn[27] is 65.8 nm), 21.3 ± 1.4 nm in width (expected width based on 2 nm DNA diameter, 1 nm interhelix gap[27] and assuming that the seed is pressed flat on mica is 17.5 nm), and 5.2 ± 0.3 nm in height. The average measured height of the seed was just larger than the height of two stacked DNA helices (typical height of double stranded DNA is 2 nm[27]), which is consistent with a cylindrical structure that is pressed flat. The unfolded region of the scaffold strand (4561 bp) could be seen on the mica surface in a random coil configuration. To confirm that the structures were cylinders, we also characterized unrolled seed origami (Figure 2b,e,h), where the staple strands that connect helix 1 and helix 12 of the cylinder (Supporting Information Figure 4) were not added to the assembly mixture. The unrolled seeds measured 65 ± 2.2 nm in length, 37.6 ± 1.0 nm in width and 2.4 ± 0.1 nm in height, that is, the same length as the fully folded seeds, but twice as wide and half as high, consistent with the idea that the fully folded seed is a cylindrical structure that is pressed flat during AFM imaging.

Nanotubes Are Bound to Seeds at the End of an Assembly Reaction. To test that tiles or nanotubes can attach to the designed seed structures, we characterized the structures that resulted when the seed, adapter, and tile strands were annealed together (Figure 2c,f,i). In previous studies, nanotubes appeared as lattices in AFM images, as the adsorption interactions between DNA and mica surface force the nanotube to open and into a flat lattice.[13] AFM images of nanotubes grown with seeds and adapter strands show seeds attached to lattices with constant widths, suggesting that the lattices are nanotubes that opened on the mica (Figure 2f). Additionally, seeded nanotubes that are enzymatically ligated remain in nanotube form upon deposition (Supporting Information Note S10). In AFM images in which 40 nM of tiles were annealed with 0.4 nM seeds, no nanotubes were observed that were not attached to seeds (N ≅ 150 tubes). Seeds (5.2 ± 0.3 nm in height) appeared brighter as compared to the tiles (2.0 ± 0.1 nm in height). There were no visible lattice distortions at the seed-tile interface.

The Presence of Seeds Increases the Number of Nanotubes That Grow and Total Nanotube Length. Our initial characterization of seeds and nanotubes showed that tiles or nanotubes can bind to the seeds. To test whether the seeds nucleate nanotubes, we next measured whether the presence of seeds increased the rate at which nanotubes appear during growth. At low supersaturation, nanotube seeds should reduce or eliminate the barrier to nanotube nucleation, resulting in the growth of more and longer nanotubes in seeded samples than in unseeded samples. We annealed nanotube tiles with and without seeds from 90 to 32 °C (low supersaturation conditions for the concentration of nanotube tiles that we used) and measured the number of nanotubes present after different incubation times at 32 °C using fluorescence microscopy (Figure 3). Nanotubes appeared much earlier and in greater numbers when the nanotube tiles were annealed with seeds as compared to without seeds: there was a 4-fold increase in the mean number of nanotubes per area for 0.004 nM seeds and a 50-fold increase for 0.04 nM seeds as compared to unseeded nanotubes after 5 h (Figure 3c). In the unseeded samples, the number of nanotubes increased throughout the 50 h we tracked. In contrast, the number of nanotubes increased steeply and then plateaued in the seeded samples, presumably because the free tile concentration dropped close to the critical concentration. The presence of seeds also affected nanotube length; at a given time, the mean length of a nanotube was

dx.doi.org/10.1021/nl400881w | *Nano Lett.* 2013, 13, 4006–4013

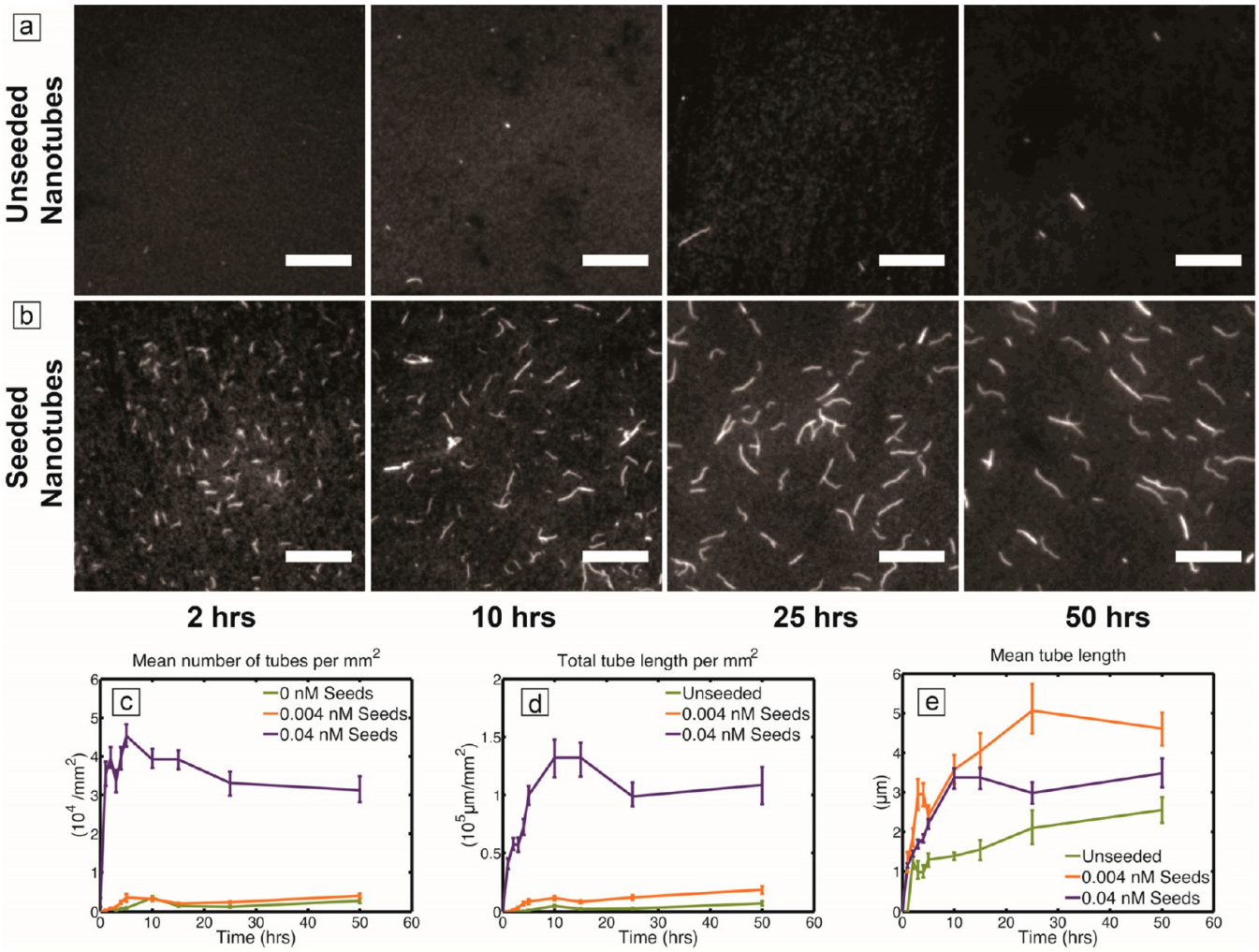

Figure 3. Seeds increase the number of nanotubes and total nanotube length. Scale bars, 10 μm. (a,b) Time course fluorescence microscopy images of nanotubes during the incubation of the sample at 32 °C. Tile concentration is 40 nM. (a) Nanotubes grown without seeds (b) Nanotubes grown with 0.04 nM seeds. (c–e) The nanotubes were measured in images like panels a and b to calculate changes in nanotube number and length with time. The error bars in the above graphs are determined by bootstrapping for 95% confidence interval.

longer in the samples with seeds than in the sample without seeds.

To further confirm that nanotubes grow rapidly because fully formed seeds are present, we first incubated nanotube tiles at 32 °C for 10 h and then added preformed seeds (see Methods). Addition of preformed seeds resulted in a rapid increase in the number of nanotubes (Supporting Information Note S15), suggesting that our seeds could be used to control nanotube growth temporally under isothermal conditions.

Tile Adapters Can Impede Nanotube Growth. Adapter tiles consisting of four adapter strands attach to one side of the seed, allowing for nanotube tiles to self-assemble on seeds and form nanotubes (Supporting Information Figure 5). To ensure that all seeds had a full set of adapter tiles, we included adapter tile strands in 100-fold excess to the scaffold strand. Hence, a lot of free adapter tiles (one-tenth the concentration of nanotube tiles) were present in solution. These free adapter tiles in solution could potentially interfere with nanotube growth as they have the structure of a nanotube tile (on one side) and the same sticky ends as tiles (see representation in Supporting Information Figure 20). The sticky ends on one side of the adapter tiles could allow them to attach easily to growing nanotubes. But because adapter tiles have sticky ends on only one side of the tile, these attached adapter tiles do not create binding sites for further tile attachment and would instead stall nanotube growth. When we grew unseeded nanotubes at 20 °C in the presence of more than 20 nM of adapter tiles, we observed a qualitative decrease in total and mean nanotube lengths, consistent with this hypothesis (Supporting Information Note S14). In our other experiments, we used adapter tile concentrations of 0.4 nM, well below the 20 nM threshold to prevent adapter tile from significantly interfering with the growth process.

Seeds Template Nanotube Circumference. AFM was used to measure the nanotube circumference by measuring the width of the lattices (in tiles) after the nanotubes opened on the surface (see Methods). When the width of this lattice varied from row to row, we assumed that the nanotube's width was the quantity most frequently observed. Using this metric, we found that nanotubes that nucleate homogeneously (without seeds) have circumferences (Figure 4a–c) ranging from 6 to 14 tiles (Figure 4d). Because the seeds provide a template for nanotubes that are 6 tiles around, we would expect that nanotubes that nucleate on seeds should have the circumference templated by the seeds. Indeed, the measured width of nanotube lattices in the seeded sample was monodisperse

dx.doi.org/10.1021/nl400881w | Nano Lett. 2013, 13, 4006–4013

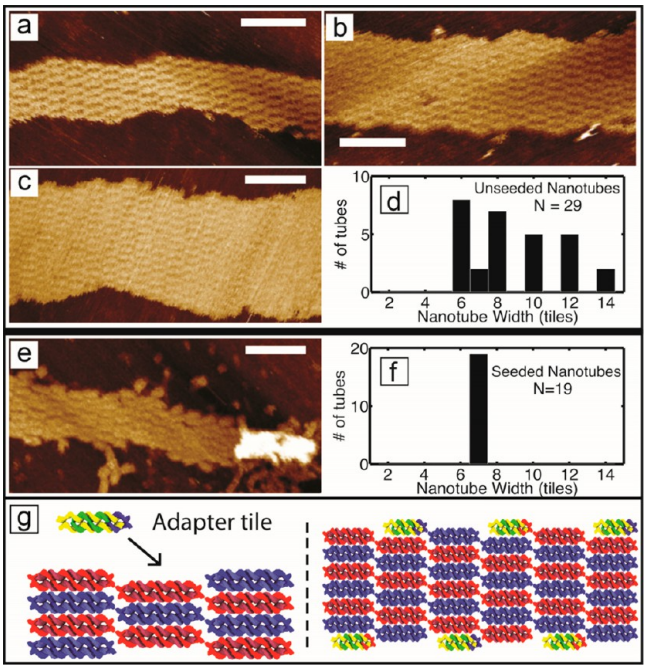

Figure 4. Seeds direct nanotube circumference. Scale bars, 50 nm. (a–c) AFM images of opened unseeded nanotubes that are 6, 10, and 14 tiles in circumference, respectively. (d) Circumference distribution of unseeded nanotubes. (e) AFM image of an opened seeded nanotube that appears to be 7 tiles wide on the surface. (f) Circumference distribution of seeded nanotubes at 0.4 nM seed concentrations. (g) Schematic diagram showing the locations of adapter tile binding sites on opened nanotubes on the mica surface. Adapter tile binding to these sites would increase the apparent width of nanotubes by exactly one tile.

(Figure 4e,f). However, all opened nanotubes observed on the mica had a majority of rows that were 7 tiles rather than 6 tiles wide on the mica surface. We expect that this width resulted from tile additions to nanotube lattices after they opened on the mica during imaging. Adapter tile interactions with nanotubes could, for example, explain the odd widths of nanotube lattices observed. Adapter tiles could bind to the edges of nanotube lattices, resulting in an increase in the apparent width of nanotubes by exactly one tile (Figure 4g, Supporting Information Note S13). We added DNA strands called "guard strands"[10] before imaging, which bind to sticky end strands of tiles and displace the sticky end strands from tiles by branch migration, therefore preventing growth of nanotubes during room temperature imaging (Supporting Information Note S4). While we used guard strands to deactivate tile-binding sites, some tiles may not have been inactivated. The observed occasional odd width in tiles of some rows in opened nanotube lattices in both the seeded and unseeded samples might also be caused by occasional binding of tiles that were not deactivated by guard strands to lattice edges. In the absence of guard strands, this type of tile attachment to nanotubes was observed previously.[13] Thus, the circumference of seeded nanotubes is consistent with templated growth from seeds followed by occasional tile attachment to opened nanotubes during imaging.

The 8-tile-circumference seeds, which template nanotubes 8 tiles in circumference (Supporting Information Notes S3 and S8), also increase the number of nanotubes that grow by 50-fold after 5 h (for 0.04 nM 8-tile seeds) but do not exert the same precise control over nanotube circumference as we observed with the 6-tile circumference seed (Supporting Information Notes S9 and S12).

The Length Distributions of Nanotubes Support Seed-Nucleated Growth When Seeds Are Present. Seeded growth should produce a different distribution of nanotube lengths than unseeded growth because seeds allow nanotubes to start growing shortly after incubation, while homogeneous nucleation is slower and occurs throughout the incubation period. We plotted histograms of the length

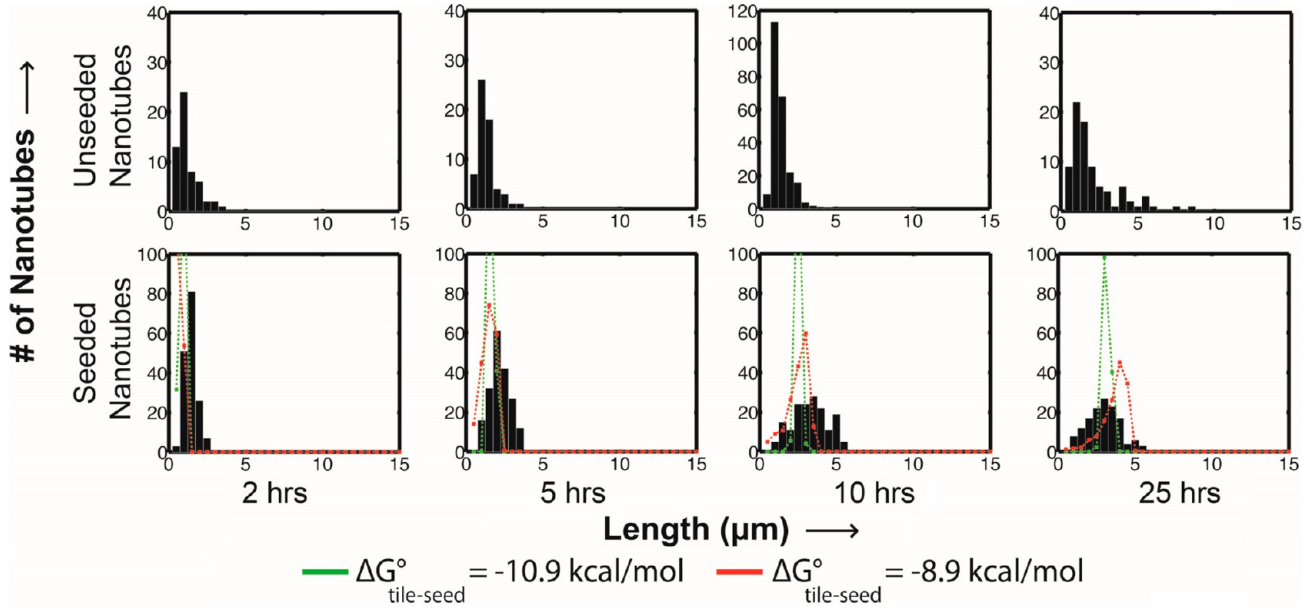

Figure 5. Length distributions of unseeded and seeded nanotubes. Length distributions of (a) unseeded nanotubes and (b) nanotubes grown with 0.4 nM seeds during 32 °C incubation. The green line plots represent the length distribution predicted in simulations. The red line is the result of simulations that include a small nucleation barrier to the attachment of tiles to seeds ($\Delta G^{\circ}_{\text{tile-seed}} = -8.9$ kcal/mol, red) as compared to attachment of tiles to existing nanotubes ($\Delta G^{\circ}_{\text{tile-tile}} = -10.9$ kcal/mol, green), representing a 25-fold difference in tile off rates from the seed.

dx.doi.org/10.1021/nl400881w | Nano Lett. 2013, 13, 4006–4013

distributions of seeded and unseeded nanotubes (Figure 5) and observed a peaked distribution in the lengths of seeded nanotubes. A peaked distribution is characteristic of templated growth because most nanotubes nucleate at the same time and grow simultaneously, allowing nanotubes to have roughly the same average lengths. In contrast, the distribution of lengths in the unseeded samples was less evenly peaked.

To learn more about the mechanisms of nucleation and growth in the two samples, we compared the experimentally observed trends in the number and length of nanotubes as well as the distributions of nanotube lengths at each time point with those predicted by stochastic kinetic simulations of nanotube growth (Supporting Information Note S16). We tried to systematically recapitulate the nanotube length distributions by using different sets of simulations in which one assembly parameter was varied.

Previously, the ΔG° of tile-assembly interaction (by two sticky ends) has been measured for DNA tile ribbons[26] and nanotubes[30] to be −10.9 kcal/mol and −10.77 kcal/mol at 32 °C, respectively. We considered how the ΔG°'s of tile interaction would affect growth rates and length distributions of seeded and unseeded DNA tile nanotubes in our experiments. Our simulations (Supporting Information Figure 24) showed that the closest match to the average seeded nanotube lengths corresponds to two sticky-end interaction strengths between −10.65 and −10.9 kcal/mol, consistent with the previous experimental measurements. However, these simulations produced distributions of nanotube lengths that were much more sharply peaked (lower variance) than the distributions we observed experimentally.

We thus considered how other factors during assembly might be responsible for the broader distributions of nanotube lengths we observed. For example, malformed tiles that can attach to nanotubes but do not provide growth sites for future tile attachments might stall growth of some nanotubes, broadening the length distribution. However, simulations that included such malformed tiles (percentages ranging up to 25% of the total tiles) do not show broader length distributions (Supporting Information Figure 26). Another assembly factor that has been previously observed as important during nanotube growth, nanotube joining, and scission,[31] could also conceivably produce a broad distribution of nanotube lengths; a single joining event between two nanotubes of equal length would produce one nanotube with twice the length, and the scission of a single nanotube in the middle could produce two nanotubes with half the length. A small number of joining and scission events could therefore potentially significantly alter the observed length distribution of nanotubes. However, our simulations found that unrealistically high rates of joining and/or scission would be required to produce experimentally observed length distributions (Supporting Information Figure 28). These simulations also showed that such high nanotube joining and scission rates are inconsistent with our experiments; under conditions with high scission rates, the number of nanotubes would increase drastically throughout the incubation period, in contrast to our observation that the number of nanotubes saturates after about 10 h (Supporting Information Figure 27). Similar simulations of the unseeded growth process (Supporting Information Figures 31−34) support our interpretations of the effects of ΔG°, malformed tiles and joining and scission on nanotube length distributions.

Previous work on nucleating DNA tile ribbons from origami found that there was a small distortion at the origami−ribbon interface,[29] suggesting that tile attachment to seeds might be less favorable than tile attachment to existing nanotubes. The result of such preference would be a small nucleation barrier to the growth of new nanotubes from seeds versus continued growth of existing nanotubes. To consider how a small nucleation barrier might have affected the growth process of nanotubes from seeds, we also modeled nanotube growth where the off rate of tiles from the seeds was significantly higher than the off rate of tiles from nanotubes ($\Delta G^\circ_{\text{tile-seed}} > \Delta G^\circ_{\text{tile−tile}}$). These simulations predicted broader distributions of nanotube lengths, consistent with our experimental observations (Figure 5, Supporting Information Figure 30). The closest fit to our experimental data for seeded nanotubes showed a $\Delta G^\circ_{\text{tile-seed}}$ of about −8.9 kcal/mol between tiles and seeds as compared to the $\Delta G^\circ_{\text{tile−tile}}$ of −10.9 kcal/mol between tiles. A higher $\Delta G^\circ_{\text{tile-seed}}$ than $\Delta G^\circ_{\text{tile−tile}}$ confirms the possibility of a higher barrier to growth of nanotubes from seeds as compared to growth from existing nanotubes. Simulations with a higher nucleation barrier to growth of nanotubes from seeds also predict the observed decrease in the mean number of nanotubes in presence of seeds after 20 h (Figure 3c, Supporting Information Figure 29). A process similar to Ostwald ripening could explain this decrease, where short nanotubes melt away and longer nanotubes keep growing due to difference in attachment rates of a tile to seed versus existing nanotubes. Finally, while scission during nanotube growth seems unlikely to be important in producing the observed distribution of nanotube lengths, scission during sample preparation through unintended rubbing of the two glass slides together could break nanotubes, effectively broadening the observed distributions.[32]

In this paper, we describe a mechanism for nucleating DNA nanotube growth using a rigid nanotube seed that is a thermally stable version of a nanotube segment. Together with work nucleating DNA nanotube ribbons,[29] this work suggests that building origami structures that are thermally stable versions of tile critical nucleus structures is a robust and versatile method for templated DNA tile nanostructure nucleation. Our assembly process allows good control of nanotube growth; nanotubes appear earlier in seeded growth than in unseeded growth and the number of nanotubes is up to 50 times greater in seeded than in unseeded samples. Careful growth of nanotubes under low supersaturation conditions means that the nanotubes grown in this study have few defects. Reducing defect rates is important because nanotube defects can affect both the structural and mechanical properties of nanotubes.[17,33] The designed seeds also allow precise control of nanotube circumference, which improves upon the performance in previous studies of templated nanotube growth.[16] This precise control of nanotube circumference lends support to the method of building a rigid nucleus as a template rather than a floppier, single-stranded structure.

Our simulations quantitatively predict the growth rates of tubes and help elucidate factors that were likely to be important in the growth process. These simulations also suggest that factors that have often been cited, such as malformed tiles (due to stoichiometric imperfections and strand synthesis errors), and higher order interactions such as joining and scission are unlikely to be significant factors affecting assembly using our protocols. They instead suggest that a small barrier to nucleation remains during growth from the template we designed and that even such a small barrier can significantly affect the distribution in length of the resulting structures.

dx.doi.org/10.1021/nl400881w | Nano Lett. 2013, 13, 4006−4013

Our experiments and simulations also identified some seed design features that could speed up nucleation and help us gain more control over nanotube growth. First, the current adapter tile design allows free adapters to interact with the nanotubes. This interaction did not significantly affect kinetics of growth at the concentrations of adapters we used, but redesign of the adapters could avoid such undersigned interactions entirely and make the assembly process more robust. A second factor that potentially reduces the performance of nanotube seeds is the small barrier to nanotube nucleation when nanotubes grow from seeds. This barrier may be due to imperfections in the seed structure as the cylinder structure was folded from a structure in which torsion could produce twist.[34] A more careful design of both the cylinder body and the tile-seed interface may reduce or eliminate this barrier.

Seeded growth could potentially be used for spatial and temporal control of nanotube nucleation, which is an important step toward our goal of achieving dynamic control over self-assembly. Spatial control of nanotube growth could be achieved by placing seeds at specific locations; we demonstrated temporal control of growth by showing that nanotubes grow rapidly only after seeds are added to a mixture of tiles. As origami structures are well-defined and modular, it would also be interesting to encompass other factors such as nanotube termination, branching, or bundling (as in the cytoskeleton) using origami to produce a wide variety of functional nanotube networks.

Methods. *DNA Nanotube and Seed Assembly Mixtures.* Tile, adapter, and seed strand sequences used in this study are listed in Supporting Information. DNA tile, adapter, and staple strands were synthesized by Integrated DNA Technologies, Inc. Adapter and tile strands were PAGE purified. The designed nanotube seed consists of a scaffold strand: (M13mp18, New England Biolabs) a 7,240 bp sequence, 72 short (54-base) staples strands, and 24 adapter strands. DNA nanotubes were labeled with Cy3 fluorescent dye to allow fluorescence imaging of nanotubes (Supporting Information Note S1). All samples were prepared in TAE buffer (40 mM Tris-Acetate, 1 mM EDTA) to which 12.5 mM magnesium acetate was added. AFM experiments to image seeded origami used 4 nM scaffold strands and 80 nM of each staple strand. In all experiments with tiles, the strands for each tile were present at 40 nM except for the strands presenting sticky ends, which were present at 80 nM to minimize the concentration of malformed tiles (Supporting Information Note S1). AFM images of seeded nanotubes used 0.4 nM scaffold strand, 16 nM of each staple strand and 4 nM of each tile adapter strand. The concentration of seeds (defined by the scaffold strand concentration) in AFM experiments was higher than in other growth experiments to ensure a sufficiently high density of seeds on the surface to measure a distribution of the circumference of nanotubes that grew from them. In fluorescence microscopy experiments, seed samples contained 15 nM staple strands and 4 nM adapter strands. We considered samples with both 0.004 and 0.04 nM of scaffold strand. Unseeded nanotube samples only contained tiles. Concentrations of tile and tile adapter strands were determined using 260 nm absorbance spectroscopy while the staple strand concentration was assumed to be that provided by IDT.

Nanotube Annealing. Samples were annealed using an Eppendorf Mastercycler in a 5-stage, one-pot reaction. Samples were first incubated at 90 °C for 5 min to melt all DNA, then annealed from 90 to 45 °C at 1 °C/min, and then incubated at 45 °C for 1 h to allow the formation of seed origami and nanotubes tiles.[29] Samples were slowly cooled from 45 to 32 °C at 0.1 °C/min to a final temperature of 32 °C, which are slightly supersaturated conditions for nanotube assembly. The nanotubes were then incubated at 32 °C.

Fluorescence Microscopy. For time course fluorescence microscopy experiments, individual samples were pipetted onto slides after different incubation times (0, 1, 2... hours) at 32 °C. To prevent growth of nanotubes during imaging or slide preparation, 2 μL of 4 μM of guard strands (Supporting Information Note S4) were added to 20 μL of 40 nM nanotube tile solution[10] and then incubated at 32 °C for 2 min. Five microliters of this solution was then transferred to an 18 mm by 18 mm glass coverslip at room temperature for fluorescence imaging. For the isothermal control of nanotube growth experiment, preformed seeds at 32 °C were added to unseeded nanotubes samples (40 nM tiles) after 10 h of incubation at 32 °C. The samples were imaged on an inverted microscope (Olympus IX71) using a 60×/1.45 NA oil immersion objective using an Olympus Cy3 filter cube set (Z532BP). Images were captured on a cooled CCD camera (iXon3, Andor).

Atomic Force Microscopy. For AFM experiments of seeded nanotubes, samples were incubated at 32 °C for 10 h. For AFM experiments of unseeded nanotubes, samples were incubated at 32 °C for a longer period (75 h) to maximize the number of nanotubes available for imaging. Before AFM imaging, 2 μL of 4 μM of guard strands were added to 20 μL of 40 nM nanotube tile solution[10] and then incubated at 32 °C for 2 min to allow the guard strands to attach to tiles and thus prevent further assembly. Five microliters of this solution in the case of seeded nanotubes, or 80 μL for unseeded nanotubes, was added onto a freshly cleaved mica surface mounted on a puck with a Teflon sheet. (More unseeded nanotube solution was required as unseeded nanotubes were sparser.) Approximately 100 μL of TAE/Mg^{2+} buffer was then added and incubated for 5 min. Images were taken after a single wash step with TAE/Mg^{2+} buffer, after which we observed cleaner images than beforethe wash (possibly due to fewer small tiles on the mica). Imaging was performed on a Dimension Icon (Bruker) using Scanasyst mode and Sharp Nitride Lever tip (SNL - 10 C, Bruker) cantilevers. Images were flattened by subtracting a linear function from each scan line using the Nanoscope Analysis software. Length and width of structures were measured using full width at half-maximum of AFM section profile. The width of a nanotube lattice on mica was not uniform along the length, due to the occasional binding of adapter tiles (in seeded samples) and tiles (in both seeded and unseeded samples) that were not deactivated by guard strands along the lattice edges. Therefore, the measured width of a nanotube lattice was taken as most frequent observed width among the lattice rows.

Measurement of Nanotube Length. For every time point at which fluorescence microscopy images of nanotubes were analyzed, we prepared three slides from a sample and captured three images from each slide. To measure the lengths of nanotubes from the images we used the ImageJ plugin "Jfilament" (http://athena.physics.lehigh.edu/jfilament/).[35] Histogram equalization was used to enhance the contrast in the fluorescence images. For seeded nanotube images, we measured nanotubes from a cropped region (1/16th of the original image area) in the top right (randomly selected) of the image, whereas the entire image area was considered for unseeded nanotube samples. Error bars in the graphs were determined by bootstrapping using a 95% confidence interval.

■ ASSOCIATED CONTENT

Supporting Information

Sequences for DNA molecules used in our experiments, additional experimental results, simulation results, and ancillary notes referred to in the paper. This material is available free of charge via the Internet at http://pubs.acs.org.

■ AUTHOR INFORMATION

Corresponding Author

*E-mail: rschulm3@jhu.edu.

Notes

The authors declare no competing financial interest.

■ ACKNOWLEDGMENTS

The authors would like to thank David Doty, Ankur Verma, and Damien Woods for helpful discussions and advice on the manuscript, Jan Liphardt for technical advice and support and Kostantinos Konstantopoulos for use of their microscopy equipment. This research was supported by NSF CCF-1161941, NSF CAREER Grant CMMI-1253876, the Miller Institute for Basic Science at U.C. Berkeley.

■ REFERENCES

(1) Close, G. F.; Yasuda, S.; Paul, B.; Fujita, S.; Wong, H. S. P. *Nano Lett.* **2008**, *8*, 706−709.

(2) Kreupl, F.; Graham, A. P.; Duesberg, G. S.; Steinhogl, W.; Liebau, M.; Unger, E.; Honlein, W. *Microelectron. Eng.* **2002**, *64*, 399−408.

(3) Chen, R. J.; Zhang, Y. G.; Wang, D. W.; Dai, H. J. *J. Am. Chem. Soc.* **2001**, *123*, 3838−3839.

(4) Dwyer, C.; Guthold, M.; Falvo, M.; Washburn, S.; Superfine, R.; Erie, D. *Nanotechnology* **2002**, *13*, 601−604.

(5) Djalali, R.; Chen, Y.; Matsui, H. *J. Am. Chem. Soc.* **2002**, *124*, 13660−13661.

(6) Gao, X. Y.; Matsui, H. *Adv. Mater.* **2005**, *17*, 2037−2050.

(7) Lo, P. K.; Karam, P.; Aldaye, F. A.; McLaughlin, C. K.; Hamblin, G. D.; Cosa, G.; Sleiman, H. F. *Nature Chem.* **2010**, *2*, 319−328.

(8) Wickham, S. F. J.; Endo, M.; Katsuda, Y.; Hidaka, K.; Bath, J.; Sugiyama, H.; Turberfield, A. J. *Nat. Nanotechnol.* **2011**, *6*, 166−169.

(9) Mao, C. D.; Sun, W. Q.; Shen, Z. Y.; Seeman, N. C. *Nature* **1999**, *397*, 144−146.

(10) Schulman, R.; Yurke, B.; Winfree, E. *Proc. Natl. Acad. Sci. U.S.A.* **2012**, *109*, 6405−6410.

(11) Feng, L. P.; Park, S. H.; Reif, J. H.; Yan, H. *Angew. Chem., Int. Ed.* **2003**, *42*, 4342−4346.

(12) Goodman, R. P.; Heilemann, M.; Doose, S.; Erben, C. M.; Kapanidis, A. N.; Turberfield, A. J. *Nat. Nanotechnol.* **2008**, *3*, 93−96.

(13) Rothemund, P. W. K.; Ekani-Nkodo, A.; Papadakis, N.; Kumar, A.; Fygenson, D. K.; Winfree, E. *J. Am. Chem. Soc.* **2004**, *126*, 16344−16352.

(14) Aldaye, F. A.; Lo, P. K.; Karam, P.; McLaughlin, C. K.; Cosa, G.; Sleiman, H. F. *Nat. Nanotechnol.* **2009**, *4*, 349−352.

(15) Mitchell, J. C.; Harris, J. R.; Malo, J.; Bath, J.; Turberfield, A. J. *J. Am. Chem. Soc.* **2004**, *126*, 16342−16343.

(16) Wilner, O. I.; Orbach, R.; Henning, A.; Teller, C.; Yehezkeli, O.; Mertig, M.; Harries, D.; Willner, I. *Nat. Commun.* **2011**, *2*, 540.

(17) Yin, P.; Hariadi, R. F.; Sahu, S.; Choi, H. M. T.; Park, S. H.; LaBean, T. H.; Reif, J. H. *Science* **2008**, *321*, 824−826.

(18) Douglas, S. M.; Chou, J. J.; Shih, W. M. *Proc. Natl. Acad. Sci. U.S.A.* **2007**, *104*, 6644−6648.

(19) Aldaye, F. A.; Palmer, A. L.; Sleiman, H. F. *Science* **2008**, *321*, 1795−1799.

(20) Bui, H.; Onodera, C.; Kidwell, C.; Tan, Y.; Graugnard, E.; Kuang, W.; Lee, J.; Knowlton, W. B.; Yurke, B.; Hughes, W. L. *Nano Lett.* **2010**, *10*, 3367−3372.

(21) Sharma, J.; Chhabra, R.; Cheng, A.; Brownell, J.; Liu, Y.; Yan, H. *Science* **2009**, *323*, 112−116.

(22) Shen, X.; Song, C.; Wang, J.; Shi, D.; Wang, Z.; Liu, N.; Ding, B. *J. Am. Chem. Soc.* **2011**, *134*, 146−149.

(23) Ding, B. Q.; Wu, H.; Xu, W.; Zhao, Z. A.; Liu, Y.; Yu, H. B.; Yan, H. *Nano Lett.* **2010**, *10*, 5065−5069.

(24) Fu, T. J.; Seeman, N. C. *Biochemistry* **1993**, *32*, 3211−3220.

(25) Winfree, E.; Liu, F. R.; Wenzler, L. A.; Seeman, N. C. *Nature* **1998**, *394*, 539−544.

(26) Schulman, R.; Winfree, E. *Proc. Natl. Acad. Sci. U.S.A.* **2007**, *104*, 15236−15241.

(27) Rothemund, P. W. K. *Nature* **2006**, *440*, 297−302.

(28) Douglas, S. M.; Dietz, H.; Liedl, T.; Hogberg, B.; Graf, F.; Shih, W. M. *Nature* **2009**, *459*, 414−418.

(29) Barish, R. D.; Schulman, R.; Rothemund, P. W. K.; Winfree, E. *Proc. Natl. Acad. Sci. U.S.A.* **2009**, *106*, 6054−6059.

(30) Hariadi, R. F.; Yurke, B.; Winfree, E. California Institute of Technology, Pasadena, CA. Personal communication, 2013.

(31) Ekani-Nkodo, A.; Kumar, A.; Fygenson, D. K. *Phys. Rev. Lett.* **2004**, *93*, 268301.

(32) Hariadi, R. F. University of Michigan, Ann Arbor, MI. Personal communication, 2013.

(33) O'Neill, P.; Rothemund, P. W.; Kumar, A.; Fygenson, D. K. *Nano Lett.* **2006**, *6*, 1379−83.

(34) Woo, S.; Rothemund, P. W. K. *Nature Chem.* **2011**, *3*, 829−829.

(35) Smith, M. B.; Li, H. S.; Shen, T. A.; Huang, X. L.; Yusuf, E.; Vavylonis, D. *Cytoskeleton* **2010**, *67*, 693−705.